Dense nitrogen-rich energetic materials: a study of 5,5'-bis(1H-tetrazolyl)amine

Authors: Dominique Laniel,[1] Elena Sebastiao,[2] Cyril Cook[2], Muralee Murugesu,[2] Anguang Hu,[3] Fan Zhang[3] and Serge Desgreniers[1]

[1]Laboratoire de physique des solides denses, University of Ottawa, Ottawa, ON, Canada K1N 6N5

[2]Department of Chemistry, University of Ottawa, Ottawa, ON, Canada K1N 6N5

[3]Defence Research and Development Canada - Suffield, 4000 Station Main, Medicine Hat, AB, Canada T1A 8K6

Abstract

5,5'-bis(1H-tetrazolyl)amine (BTA), a nitrogen rich molecular solid has been investigated under compression at room temperature. Powder x-ray diffraction using synchrotron radiation and micro-Raman spectroscopy were carried out to pressures up to 12.9 GPa. BTA conserves the crystalline structure of its room condition phase up to the highest pressure, i.e., an orthorhombic unit cell (*Pbca*). A fit of the isothermal compression data to the Birch-Murnaghan equation of state reveals the high compressibility of BTA. An analysis of the volume change with pressure yields a bulk modulus and its derivative similar to that of high-nitrogen content molecular crystals. Upon laser heating to approximately 1100 K, the sample decomposed while pressurized at 2.1 GPa, resulting in a graphitic compound. Finally, numerical simulations demonstrate that the minimum energy conformation is not experimentally observed since a higher energy conformation allows for a more stable dense packing of the BTA molecules.

Introduction

Much effort has been devoted to the synthesis of novel high density energetic compounds which could be more efficient than current ones. Nitrogen-based energetic materials are in that regard promising candidates.[1-3] In the pure state, a very large energy difference is expected between molecular nitrogen

triple bond (954 kJ/mol) and that of a single bond (160 kJ/mol) configuration.[4] The former molecular state is thermodynamically favored. Among all high density energetic materials, a single-bonded nitrogen network (often referred to as polymeric nitrogen) would be, however, the material that could release the most energy upon a transition to the normal ground state. In addition, single-bonded nitrogen would have the advantage of being environmentally friendly, as its diatomic standard gaseous state (N_2) would be obtained as the final product.[5] Dense nitrogen has been observed to form an extended solid, namely cubic-gauche nitrogen (cg-N), under high static compression and high temperature.[6] Polymeric or cubic-gauche nitrogen, however, has not yet been retrieved at ambient pressure. Other avenues to attain novel energetic materials with high energy density need to be explored. Nitrogen-rich carbon nitride materials are promising alternatives as they have been shown, through simulations, to achieve extended structures potentially metastable at ambient conditions.[5] Carbon-nitrogen materials present other interesting characteristics. For instance, numerical simulations have indicated that a single-bonded network of carbon and nitrogen atoms could form a very hard material, surpassing diamond in that regard.[7-8]

In this paper, we present observations on high-density 5,5'-bis(1H-tetrazolyl)amine (BTA), a nitrogen-rich carbon nitride with an orthorhombic (*Pbca*) unit cell (Fig. 1). As a high nitrogen content material based on tetrazoles, BTA is of interest for its high heat and temperature of decomposition as well as for other relevant propulsion parameters, as calculated by Klapötke and Stierstorfer.[9] BTA samples were isothermally compressed at 300 K in a diamond anvil cell (DAC), up to a pressure of 12.9 GPa. Micro-Raman spectroscopy and powder x-ray diffraction experiments were carried out to study the change in vibrational properties and unit cell parameters with pressure, respectively, and monitor any possible pressure induced structural transitions. Following this study, we report no phase transition in dense BTA up to the maximum pressure, namely 12.9 GPa. Subtle structural deformations, however, have been observed. Finally, laser heating of a BTA sample compressed in a DAC at 2.1 GPa was also performed and the resulting product was characterized. As a complement, we have carried out

computational simulations of the lowest energy molecular conformations and vibrational properties at room conditions.

Experimental method and computational analysis

Polycrystalline BTA was obtained from BTA monohydrate. BTA monohydrate was prepared according to the procedure outlined by Klapötke *et al*.[10] Crystals of BTA monohydrate were recovered through a supersaturated solution of methanol. They were then dehydrated under vacuum for 48h at 150°C with a P_2O_5 trap resulting in good quality BTA powder. The purity of the sample was confirmed using IR and Raman spectroscopy, NMR and x-ray diffraction measurements, and by comparing the results to previously published data.[10] The BTA sample was stored under nitrogen atmosphere until used.

For micro-Raman spectroscopy and powder x-ray diffraction experiments, polycrystalline BTA, neon, and a ruby microsphere were loaded in a ~ 100 μm diameter hole of a pre-indented rhenium gasket of a diamond anvil cell (DAC). The ruby microsphere was used for *in-situ* pressure measurements, using the R_1-luminescence line as a pressure gauge[11] and using width of the R_1 and R_2 lines as an indicator of the hydrostaticity prevailing in the compression chamber. Pressure uncertainties are estimated as ± 0.03 GPa. The diamond anvils were of type Ia, with a flat culet of either 200 or 300 μm in diameter. Neon, which allows quasi-hydrostatic pressures up to 16 GPa[12] was used as inert pressure transmitting medium. Neon was loaded as a high pressure gas along with the BTA sample and the ruby microsphere into the DAC. The sample purity after loading was assessed by Raman spectroscopy. Micro-Raman spectroscopy was carried out on a BTA sample pressurized up to 11.9 GPa by increments of about 0.5 GPa. Raman scattering was induced using an argon ion laser (488 nm) with an estimated maximum power of 100 mW at the sample, and detected in near-backscattering geometry employing an Iridian Rayleigh scattering edge filter with an Andor 0.5 m spectrograph equipped with a Peltier-cooled charge-coupled device (CCD) detector. The spectral resolution of this setup was 1.7 cm^{-1} using an 1800 g/mm holographic diffraction grating. Pressure was measured before and after each acquisition.

Angle-dispersive powder x-ray diffraction measurements were carried out using synchrotron radiation at the Hard X-ray MicroAnalysis (HXMA) 06ID-1 Beamline at the Canadian Light Source (CLS). The synchrotron radiation at the HXMA beamline originated from a 63-pole superconducting wiggler. A wavelength of 0.50918 Å (24.350 keV) was set employing a double-crystal silicon (111) monochromator. The x-ray beam was collimated down to 30 μm. Details of the experimental setup are described elsewhere.[13] Typical exposure times were 20-30 min. For the x-ray diffraction experiments, the BTA samples were pressurized up to 12.9 GPa, with steps of about 0.5 GPa. Pressure was measured before and after each measurement. FIT2D[14] was utilized to process and integrate the x-ray diffraction images in order to obtain intensity vs 2θ patterns. These patterns were further analyzed and indexed using the XRDA software.[15] MAUD software[16] was used to refine the lattice parameters of the ambient x-ray diffraction pattern. Lattice parameters at each pressure were estimated to ± 0.01 Å giving uncertainties for the unit cell volume of ± 0.03 $Å^3$.

A 1070 nm fiber laser (SPI Lasers) was employed to perform laser heating on a BTA sample in a DAC compressed to 2.1 GPa. While heated, the BTA sample emitted strong incandescent light from which a temperature of 1100±100˚C was estimated based on the analysis of blackbody radiation. Laser heating resulted in darkening of the sample. To further characterize the product obtained from laser heating, micro-Raman spectroscopy was achieved on both the dark and bright areas of the unloaded sample, using a Renishaw In Viva Raman instrument with a 785 nm excitation laser.

To complement our experimental results we also carried computational work on BTA. All numerical calculations were based upon density functional theory (DFT) within the generalized gradient approximation (GGA).[17] To study the BTA molecule conformations under normal conditions, DFT calculations were carried out using GAMESS[18] at the B3LYP density functional and 6-31G(d, p) basis set level theory. The vibrational properties of BTA were characterized using the same density functional and basis set level theory. The resulting vibrational frequencies were scaled by 0.961 in accordance with conventional DFT practices.[19] For the room-temperature vibrational density of state in the condensed

phase, the SIESTA[20] calculations were performed using Troullier-Martins norm-conserving pseudopotential.[21] The room-temperature vibrational density of state was obtained from velocity auto-correlation functions of molecular dynamic simulations at 300 K and 0 GPa. Bond and angle displacements were used to make assignments of vibrational modes.

Results and discussion

High pressure X-ray diffraction

At ambient conditions, the powder x-ray diffraction pattern of BTA is in good agreement with that found in the literature.[10] Using MAUD, a refinement was performed on the ambient conditions x-ray diffraction pattern to obtain the unit cell parameters (see Fig. 2); those were corroborated by a refinement done in XRDA. The unit cell parameters obtained (see Table I) are slightly higher than those in Ref. 9. This is expected since the x-ray diffraction patterns were taken with a temperature difference of 93 K. Thermal expansion easily accounts for the small difference in the values of the unit cell parameters measured in this study.

The unit cell parameter determination at each pressure was achieved using at least 10 diffraction lines, namely (020), (021), (121), (213), (204), (214), (106), (223), (313) and (304). These diffractions lines are shown in the inset of Fig. 2. The sharpest and most intense diffraction lines are between 6 and 10 degrees. Selected x-ray diffraction patterns are shown in Fig. 3. The change of *d*-spacings as a function of pressure is displayed in Fig. 4. The overall intensity of the BTA diffraction lines steadily decreases as the pressure increases, due to sample thinning. The x-ray diffraction patterns recorded at 3.0 and 4.5 GPa show a broad intensity centered at $2\theta \sim 13$ degrees, which arises from scattering due to liquid neon. After neon solidifies at 4.6 GPa,[22] two Ne x-ray diffraction lines appear,[23] as well as one weak BTA diffraction line at $2\theta \sim 12.5$ degrees. The new BTA x-ray diffraction line is overlapped at lower pressure by the liquid neon x-ray scattering; it should be noted that it was present in the x-ray diffraction pattern obtained at ambient pressure. This line merges with another BTA diffraction line around 7 GPa. The two new neon

diffraction lines are pointed out by lozenges (◊) in Fig. 3. Rhenium (gasket) diffraction lines are also present in the pattern. They are marked in Fig. 3 by an asterisk (*) and are easily identified by their smaller shift towards higher 2θ values as pressure increases, given the relatively low compressibility of Re. In Fig. 4, at 4.5 GPa and 2θ ~ 9.0 degrees (*d*-spacing = 3.3 Å), the (222) BTA diffraction line is well separated from the (106) line. The (222) diffraction line is easily identified at 6.6 GPa and at 2θ = 9.1 degrees (3.2 Å) in Fig. 3. Its corresponding *d*-spacing and intensity decrease faster with pressure than the (106) diffraction line, and it can no longer be differentiated from the incoherent scattering background at 8.4 GPa. The smooth and continuous progression of the various diffraction lines as well as the lack of appearance of new diffraction lines indicate the absence of a phase transition in BTA up to the measured pressure.

Based on the relative change of unit change volume, shown in Fig. 5(b), BTA proves to be very compressible, with a decrease in volume of 22% from ambient pressure to 12.9 GPa. The third-order Birch-Murnaghan equation of state was used to calculate the bulk modulus and its derivative. A refinement to the volume data yielded values of B_0 = 11.8(4) GPa; B_0' = 16(1). These values are similar to other large molecular crystals, such as α-RDX (B_0 = 10.0(5) GPa; B_0' = 11.3(7)),[24] β-HMX (B_0 = 12.4 GPa; B_0' = 10.4)[25] and LLM-105 (B_0 = 11.19(2) GPa; B_0' = 18.54(4)).[26] It is interesting to note the anisotropic behavior of BTA under compression. As indicated in Fig. 5(a), the *a*-axis is the most compressible, followed by the *c*-axis and the *b*-axis, the latter being only mildly compressible.

High pressure micro-Raman spectroscopy

BTA, being a crystalline solid of space group *Pbca* (61) with atoms only on the 8c Wyckoff sites, possesses 36 Raman active vibrational modes. 24 of these 36 Raman-active vibrational modes were observed in this study. The Raman spectrum obtained at ambient conditions is very similar to that reported previously.[10] Table II presents a summary of the numerically calculated mode frequencies corresponding to Raman active vibrational modes and their assignment in comparison with the

experimentally observed Raman lines. The numerical simulations indicate intense peaks at about 3594, 3631 and 3656 cm^{-1} that were not observed experimentally due to a strong photo induced luminescent signal at high wavenumbers in our samples. This strong luminescence is also the reason why the Raman line calculated at 2986(58) cm^{-1} was not observed in this study, although present in Ref. 10. Klapötke *et al.*[10] used a 1064 nm excitation laser, which reduces luminescence. All 21 other Raman lines reported[10] are observed from our sample; additionally we have observed 20 additional Raman lines not detailed in Ref. 10. In Table II, calculated Grüneisen parameters are listed where a suitable number of pressure points were recorded. In general, as expected for molecular crystals, low mode frequencies correlate with larger Grüneisen parameters. Modes with higher frequencies (intramolecular vibrations) present lower Grüneisen parameters (see Supplementary Material for details).[27]

Fig. 6 shows selected Raman spectra obtained up to 12.0 GPa. There is a smooth and continuous transition of the vibrational mode frequencies, with a continuous decrease of Raman line intensity and width, as estimated by the full width at half maximum. At 12.0 GPa, due to the thinning of the sample and increase luminescence background, the signal intensity for most peaks is weak. At higher pressure, the Raman signal intensity has become too weak to yield reliable information. The progression of each Raman lines as a function of pressure is plotted in Fig. 7. As expected from the x-ray diffraction results, all peaks continuously and smoothly increase in wavenumber as pressure is increased. Because of the monotonous increase of the Raman shifts and the lack of any additional vibrational lines, we conclude that there is no phase transition occurring up to 12.0 GPa. This result corroborates the conclusion drawn from the x-ray diffraction pattern analysis. Furthermore, from the change of Raman mode frequencies, it is concluded that BTA molecules are stable and no strong molecular interaction arises as a function of pressure.

Conversion of dense BTA at high temperature

BTA was heated, using near-infrared laser radiation, while still pressured at 2.1 GPa in a DAC. The modification introduced by the laser heating, i.e. the darkening of the sample, is seen in the photomicrograph of the recovered BTA sample (inset of Fig. 8). Raman spectroscopy was performed on both the non-heated (bright) and the laser heated (dark) areas of the recovered sample (see Fig. 8). The Raman spectrum of the dark region of the sample is very luminescent, but nevertheless shows a double band centered at 1446 cm^{-1}. The doublet corresponds to the G-band of graphitic compounds.[28] Thus, laser-induced decomposition of BTA occurred, wherein all nitrogen-carbon bonds have been broken. Upon recovery of the sample at ambient conditions, no vibrational line for nitrogen gas was recorded in the spectrum. The Raman spectrum of the bright and unmodified area is in agreement with the spectrum of BTA at ambient pressure.

Quantum theory simulations

As pointed out in Ref. 10, numerical calculations show that the energy minimization conformation of the BTA molecule at room temperature and ambient pressure is slightly different than experimentally observed under the same conditions. Starting from its conformation of the condensed phase at ambient conditions, simulations showed that one tetrazole molecule can rotate towards its energy minimization conformation in which the spatial orientations of two tetrazole molecules with the respect to the plane of -C-NH-C- amine group is 180° (seen in Fig. 9). Thus in the condensed phase, some hydrogen atoms are not located at the expected positions. To pack BTA molecules into its condensed phase, however, hydrogen bonding plays a role in stabilizing the whole system. This requires that all hydrogen atoms be located at the same side of BTA molecules, pointing to the atoms of neighbouring molecules. In this way, stable zigzag belts are formed at the condensed phase for the dense packing (seen in Fig. 1(b)).

Conclusion

The present study puts forward the results of x-ray diffraction measurements and micro-Raman spectroscopy of dense BTA obtained by the application of quasi-hydrostatic pressures up to 12.9 GPa and

at room temperature. Our results indicate no obvious structural phase transition in BTA up to the measured pressure. Theoretical Raman vibrational mode frequencies and their corresponding molecular motion were calculated and are in good agreement with the experimental work. 21 previously unreported Raman lines were identified at ambient conditions. A structure refinement was performed on the x-ray diffraction pattern at ambient conditions. Taking into account the thermal expansion, the yielded lattice parameters are in excellent agreement with previously reported values.[10] The bulk modulus of BTA was calculated using the third-order Birch-Murnaghan equation of state, and values of $B_0 = 11.8(4)$ GPa and $B_0' = 16(1)$ were obtained. Laser heating was performed on a BTA sample pressurized at 2.1 GPa in a DAC, resulting in the decomposition of the molecular assembly and corresponding to highly-luminescent graphitic compounds. Finally, our numerical simulations showed that the non-minimum energy conformation of the BTA molecule was more favorable for dense packing, hence why it is experimentally observed.

Acknowledgments

D. L. and S. D. acknowledge the financial support of the Natural Sciences and Engineering Research Council of Canada and of the Defense Threat Reduction Agency. Portions of the described research in this paper was performed at the Canadian Light Source, which is funded by the Canada Foundation for Innovation, the Natural Sciences and Engineering Research Council of Canada, the National Research Council Canada, the Canadian Institutes of Health Research, the Government of Saskatchewan, Western Economic Diversification Canada, and the University of Saskatchewan. D. L. acknowledges the travel support from the Canadian Light Source. The authors gratefully acknowledge the work of Dr. Ning Chen, Chang-Yong Kim and Weifeng Chen in facilitating experiments carried out at the HXMA beamline of the Canadian Light Source. Authors also thank Dr. Jason Maley from the Saskatchewan Structural Science Centre for his contribution to the near-infra Raman spectra shown in this article.

References

1. V. E. Zarko, Combust., Expl., Shock Waves, **46**, 121 (2010).

2. A. Bhattacharya, Y. Q. Guo and E. R. Bernstein, J. Chem. Phys. **131**, 194304 (2009).

3. Y. Huang, Y. Zhang and J. M. Shreeve, Chem. Eur. J. **17**, 1538 (2011).

4. J.A. Ciezak, Army Research Laboratory Technical Report No. **ARL-TR-**4478, 2008.

5. A. Hu and F. Zhang. J. Phys.: Condens. Matter **22**, 505402 (2010).

6. M. I. Eremets, A. G. Gavriliuk, I. A. Trojan, D. A. Dzivenko and R. Boehler, Nature Mater. **3**, 558 (2004).

7. A. Y. Liu and M. L. Cohen, Science **245**, 841 (1989).

8. D. M. Teter and R. J. Hemley, Science **271**, 53 (1996).

9. T. M. Klapötke and J. Stierstorfer. Document ADA504339. www.dtic.mil/cgi-bin/GetTRDoc?AD=ADA504339.

10. T. M. Klapötke, P. Mayer, J. Stierstorfer and J. J. Weigand, J. Mater. Chem. **18**, 5248 (2008).

11. A. Dewaele, M. Torrent, P. Loubeyre and M. Mezouar, Phys. Rev. B **78**, 104102 (2008).

12. M. Eremets, in *High Pressure Experimental Methods* (Oxford Science Publications, New York, 1996), p. 186.

13. J.S. Smith and S. Desgreniers, J. Synchrotron Rad. **16**, 83 (2009).

14. A. P. Hammersley, S. O. Svensson, M. Hanfland, A. N. Fitch and D. Häusermann, High Press. Res. **14**, 235 (1996).

15. S. Desgreniers and K. Lagarec, J. Appl. Crystallogr. **27**, 432 (1994).

16. L. Lutterotti, S. Matthies and H. R. Wenk, IUCr: Newsletter of the CPD **21**, 14 (1999).

17. J. P. Perdrew and M. Ernzerhof, Phys. Rev. Lett. **77**, 3865 (1996).

18. M. W. Schmidt, K. K. Baldridge, J. A. Boatz, S. T. Elbert, M. S. Gordon, J. H. Jensen, S. Koseki, N. Matsunaga, K. A. Nguyen, S. Su, T. L Windus, M. Dupuis and J. A. Montgomery, J. Comput. Chem. **14**, 1347 (1996).

19. R. S. McWilliams, Y. Kadry, M. F. Mahmood, A. F. Goncharov and J. Ciezak-Jenkins, J. Chem. Phys. **137**, 054501 (2012).

20. J. Soler, E. Artacho, J. Gale, A. Garcia, J. Junquera, P. Ordejon and D. Sanchez-Portal, Phys.: Cond. Matt. **14**, 2745 (2002).

21. N. Troullier and J. Martins, Phys. Rev. B **43**, 1993 (1991).

22. H. Shimizu, H. Imaeda, T. Kume and S. Sasaki, Phys. Rev. B **71**, 104108 (2005).

23. R. J. Hemley, C. S. Zha, A. P. Jephcoat, H. K. Mao and L. W. Finger, Phys. Rev. B **39**, 11820 (1989).

24. I. D. H. Oswald, D. I. A. Millar, A. J. Davidson, D. J. Francis, W. G. Marshall, C. R. Pulham, A. Cumming, A. R. Lennie and J. E. Warren, High Pressure Res. **30**, 280 (2010).

25. C.-S. Yoo and H. Cynn, J. Chem. Phys. **111**, 10229 (1999).

26. J. C. Gump, C. A. Stoltz, B. G. Freedman and S. M. Peiris, AIP Conf. Proc. **1195**, 541 (2009).

27. See supplemental material at [URL will be inserted by AIP] for additional Figures and Table.

28. A. C. Ferrari and J. Robinson, Phil. Trans. R. Soc. Lond. A **362**, 2477 (2004).

Figure captions:

Fig. 1. (a) Asymmetric unit cell of BTA. (b) Orthorhombic (*Pbca*) unit cell of BTA.

Fig. 2. Calculated (dotted line) and experimentally observed (solid line) x-ray diffraction patterns of BTA, at ambient conditions. Vertical tick marks indicate reflection positions for the orthorhombic (*Pbca*) structure of BTA. The inset provides an enlargement of the 6 to 10 degree range, along the 2θ axis. With the exception of line (312), the *hkl* values are the ones that were used to obtain the lattice parameters. Note that x-ray diffraction patterns are background corrected.

Fig. 3. X-ray diffraction patterns at selected pressures. An offset on the vertical axis was used to improve clarity. The broad intensity centered at 2θ ~ 13 degrees at 3.0 and 4.5 GPa results from the scattering due to liquid neon, which, upon solidifying, introduces additional lines that are marked by a lozenge (◊). Asterisks (*) indicate a rhenium diffraction line. Due to sample thinning, the intensity steadily decreases with pressure. Aside from Ne peaks, no new peaks arise from the sample, indicating no phase change.

Fig. 4. The changes of *d*-spacing as a function of pressure for BTA. The smooth and continuous *d*-spacing shifts with pressure, indicating no obvious structural phase change. Points corresponding to the x-ray diffraction lines of neon and rhenium were omitted.

Fig. 5. (a) Normalized lattice parameters with respect to pressure. (b) The pressure with respect to the normalized volume, fitted with the third-order Birch-Murnaghan equation of state, yielded B_0 = 11.8(4) GPa and B_0' = 16(1). The data in a) and b) were normalized using the lattice parameters (a_0 = 11.26(1) Å; b_0 = 9.24(1) Å; c_0 = 21.34(1) Å) and the volume (V_0 = 2220.26(3) Å^3) at ambient pressure, respectively.

Fig. 6. Raman spectra of BTA at selected pressures. Overall, the lack of new peaks indicates that there was no phase transition up to the maximum pressure. The sharp and intense Raman line at 1330 cm^{-1} is from the diamond anvils of the DAC.

Fig. 7. Pressure dependant shift of Raman modes of BTA. The smooth and continuous peak displacement indicates no phase change.

Fig. 8. Raman spectra of the laser heated and non-heated regions of the BTA sample. For clarity, a *y*-axis offset was applied. The Raman spectrum from the non-heated area corresponds to the ambient spectrum of BTA, in spite of the superimposed luminescence. The Raman spectrum recorded on the laser-heated area corresponds likely to a graphitic compound, resulting from the photo-induced decomposition of the BTA sample. Inset: Photomicrograph of a recovered BTA sample. a) non-heated BTA. b) heated BTA; the sample was displaced while heated, thus giving us a dark line instead a spot.

Fig. 9. Simulations showed that one tetrazole molecule can rotate towards its energy minimization conformation; (a) the initial conformation from the condensed phase at ambient conditions, (b) the intermediate conformation in which the planes of two tetrazoles are perpendicular, (c) the final conformation in which the planes of two tetrazoles are 180°.

List of tables:

Table I. Structural properties of BTA at ambient pressure. The lattice parameters and their uncertainty were obtained by refining our data using MAUD.

	Klapötke *et al.*[10]	This study
a (Å)	11.109(2)	11.26(1)
b (Å)	9.227(2)	9.24(1)
c (Å)	21.327(4)	21.34(1)
V (Å^3)	2186.1(7)	2220.26(3)
T (K)	200	293

Table II. Mode frequencies (in cm^{-1}) of observed Raman lines compared with previously reported spectral lines[10] at ambient pressure. Numerically calculated vibrational modes (and intensity, in Å^4/AMU) and their corresponding molecular motion are based on the DFT model described in the text. '—' indicates

that the corresponding vibrational mode was not followed as a function of pressure and therefore a Grüneisen parameter was not calculated.

This work	Klapötke *et al.*[10] (intensity)	Calculated	Grüneisen parameter	Molecular motion
59		57	1.24	ρ $(CHN_4)_2$ (two tetrazole rings)
68			2.52	Overtone/combination
72			1.90	Overtone/combination
82		85	—	τ $(CHN_4)_2$ (two tetrazole rings)
89			1.38	Overtone/combination
102			2.05	Overtone/combination
117			1.55	Overtone/combination
141		135	1.27	δ$(CHN_4)_2$ (two tetrazole rings)
154			—	Overtone/combination
165	167(47)		1.79	Overtone/combination
196	201(41)		0.95	Overtone/combination
		262		ω$(CHN_4)_2$ (two tetrazole rings)
310	312(26)	316	0.46	ρ$(CHN_4)_2$ (two tetrazole rings)
339	339(32)	328	0.07	δ$(CHN_4)_2$ (two tetrazole rings)
347		350	0.21	τ $(CHN_4)_2$ (two tetrazole rings)
367		373	0.26	ρ$(CHN_4)_2$ (two tetrazole rings) or overtone/combination
367		373	0.50	ρ$(CHN_4)_2$ (two tetrazole rings) or overtone/combination
388			0.34	Overtone/combination
395	397(81)		0.43	Overtone/combination
		458		τ NH
		605		τ NH

		678		τ H-N-N-N
		695		τ C-N-N-N
		703		τ C-N-N-N
732		724	0.01	τ H-N-N-N
789		756	—	ρ $(CHN_4)_2$ (two tetrazole rings)
810	810(13)	801	—	ω$(CHN_4)_2$ (two tetrazole rings)
846			0.82	Overtone/combination
		955		ω H-N-N-N
		965		ω H-N-N-N
		977		ω H-N-N-N
994		990	—	ν H-N-N
1000			0.17	Overtone/combination
1015	1014(38)	1033	0.15	ν H-N-N
1056	1057(53)	1044	0.03	ν H-N-N
1068			—	Overtone/combination
1077	1078(50)	1073	0.10	ν N-N
1088			0.15	Overtone/combination
1100		1101	0.22	ν N-N
1124			0.03	Overtone/combination
1131	1132(100)		0.14	Overtone/combination
1143			0.22	Overtone/combination
1150			0.19	Overtone/combination
1184	1186(57)	1213	0.12	ν H-N-N
1226	1243(17)	1230	0.07	ν H-N-N
1284	1287(27)	1292	0.03	ν H-N-C or overtone/combination

1284	1287(27)	1292	0.14	ν H-N-C or overtone/combination
1319	1322(38)		—	Overtone/combination
1327		1330	—	τ H-N-N-N
1377	1381(37)	1364	1.06	ν N-C-N
1419	1422(20)		0.05	Overtone/combination
1448	1450(32)	1434	0.08	ν N-C-N
1458		1490	0.11	δ C-N-H
1548	1550(83)		0.11	Overtone/combination
1566	1568(22)	1553	0.08	δ C-N-H
1592	1595(48)		0.14	Overtone/combination
1603			0.11	Overtone/combination
1609	1606(47)	1609	0.14	δ C-N-H
1674			0.11	Overtone/combination
	2986(58)			Overtone/combination
		3454		ν H-N
		3490		ν H-N
		3514		ν H-N

τ, Torsional; δ, bending; ω, wagging; ν, stretch.

(a)

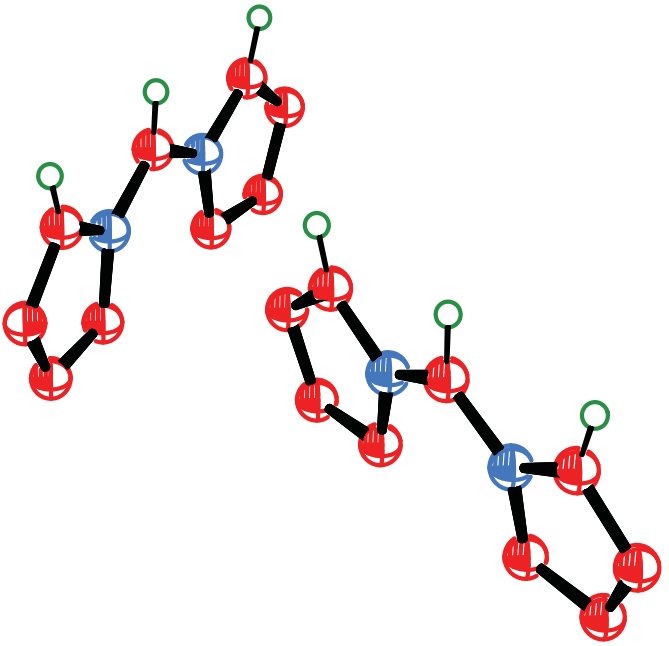

(b)

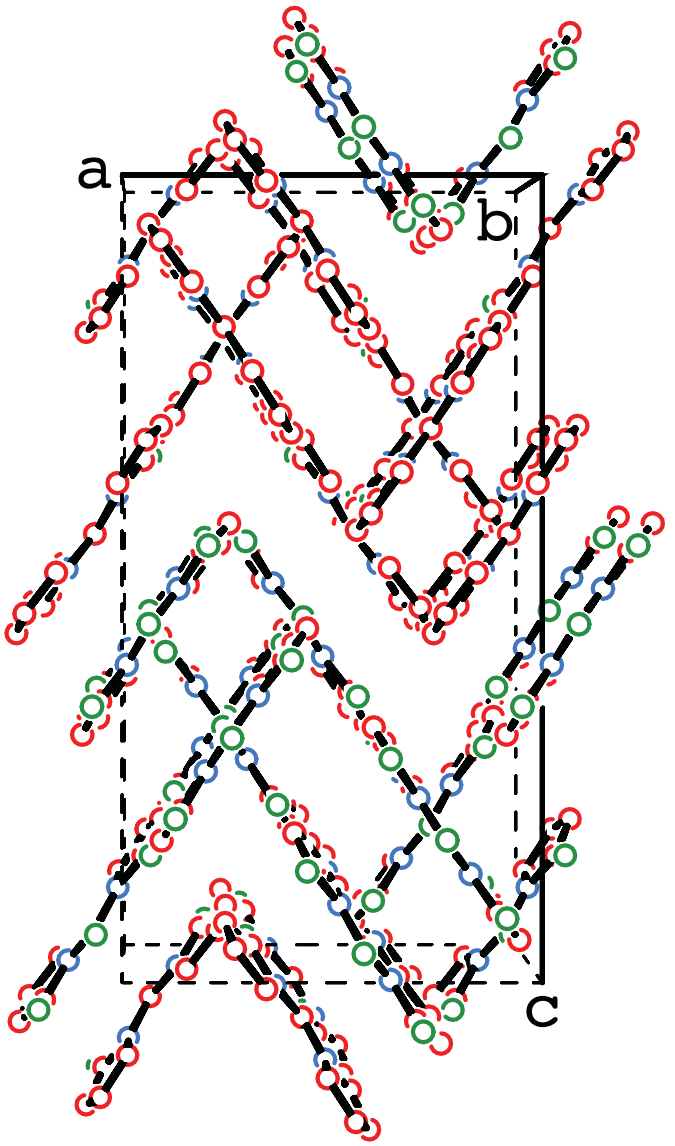

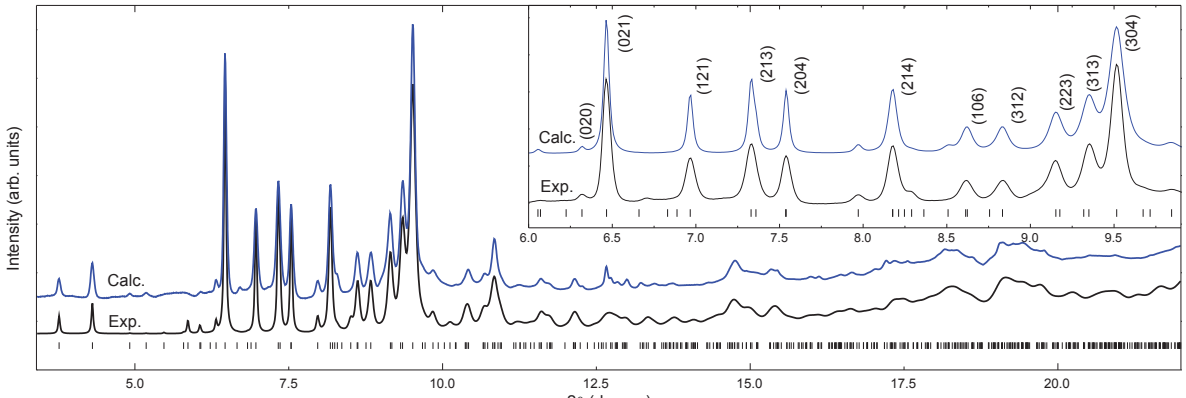
Intensity (arb. units)
Calc.
Exp.
5.0
7.5
10.0
12.5
15.0
17.5
20.0
2θ (degree)
(020)
(021)
(121)
(213)
(204)
(214)
(106)
(312)
(223)
(313)
(304)
Calc.
Exp.
6.0
6.5
7.0
7.5
8.0
8.5
9.0
9.5

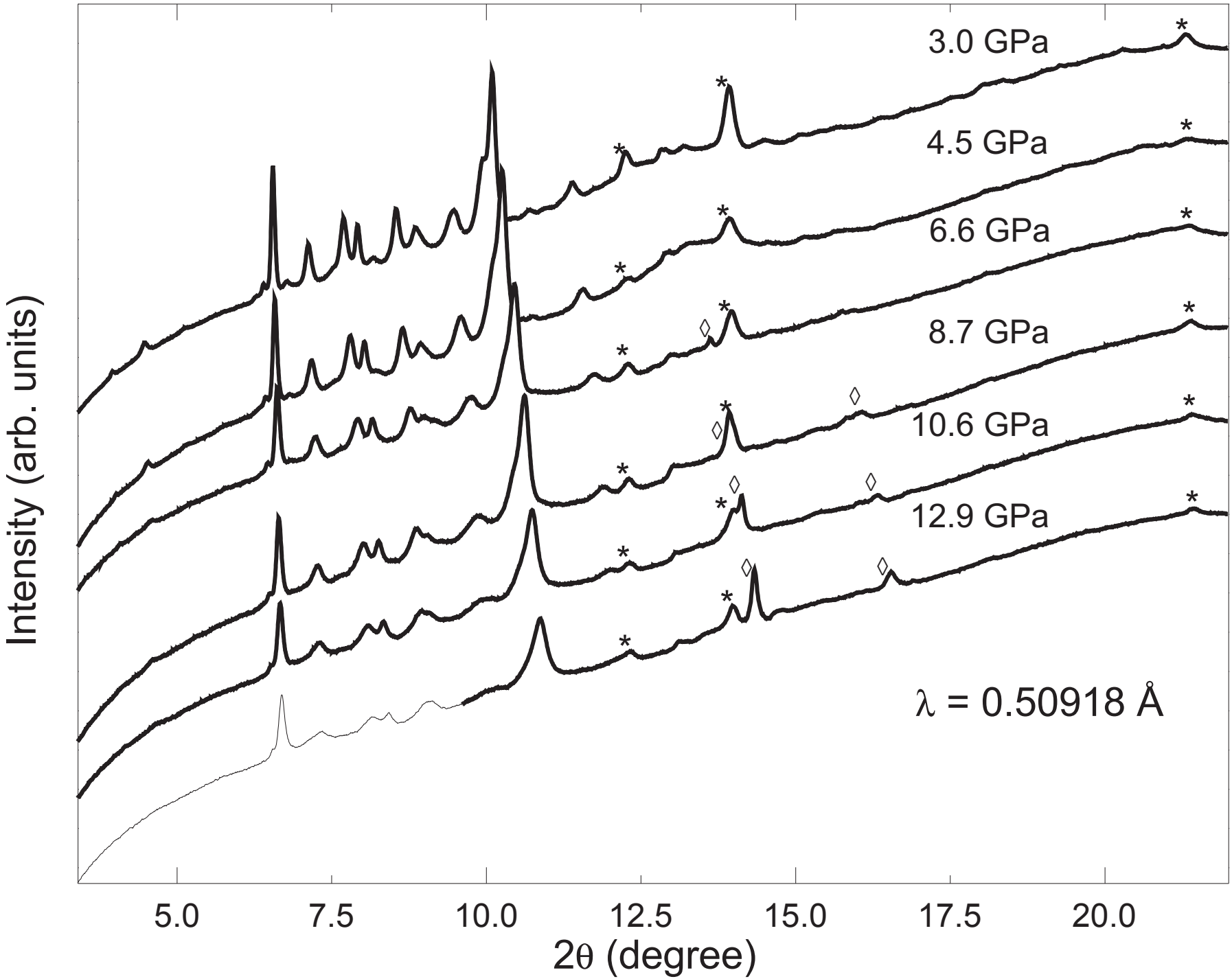
3.0 GPa
4.5 GPa
6.6 GPa
8.7 GPa
10.6 GPa
12.9 GPa
λ = 0.50918 Å
Intensity (arb. units)
2θ (degree)
5.0
7.5
10.0
12.5
15.0
17.5
20.0

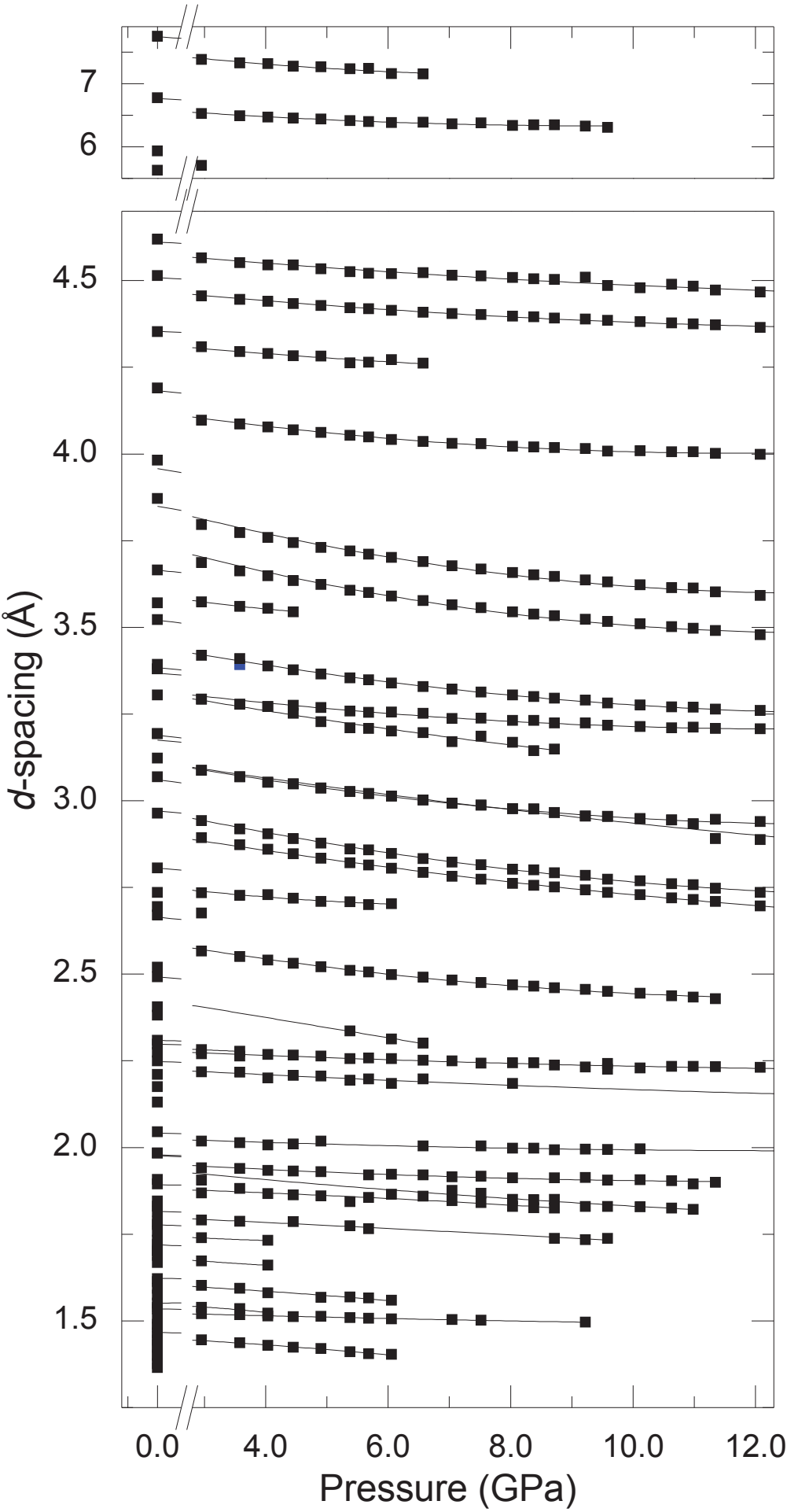
7
6
4.5
4.0
3.5
3.0
2.5
2.0
1.5
d-spacing (Å)
0.0
4.0
6.0
8.0
10.0
12.0
Pressure (GPa)

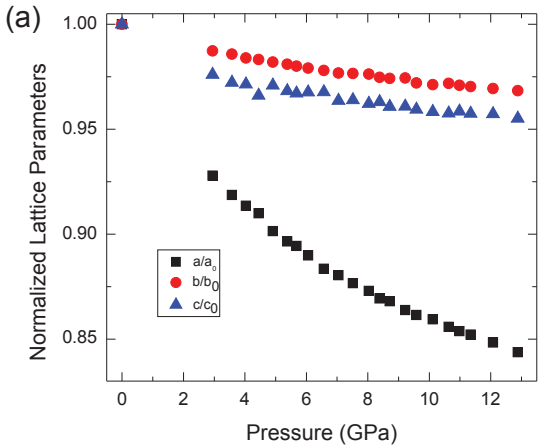
(a)
Normalized Lattice Parameters
1.00
0.95
0.90
0.85
a/a0
b/b0
c/c0
0
2
4
6
8
10
12
Pressure (GPa)

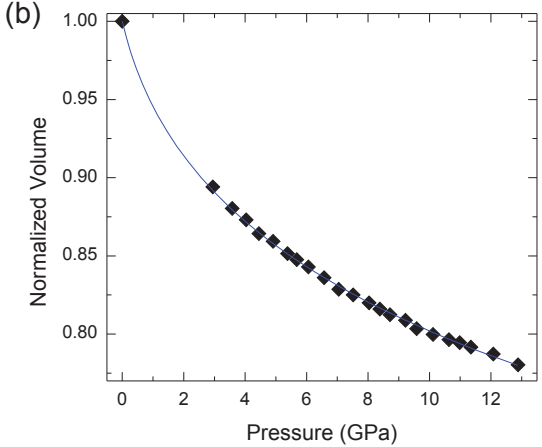
(b)
Normalized Volume
1.00
0.95
0.90
0.85
0.80
0
2
4
6
8
10
12
Pressure (GPa)

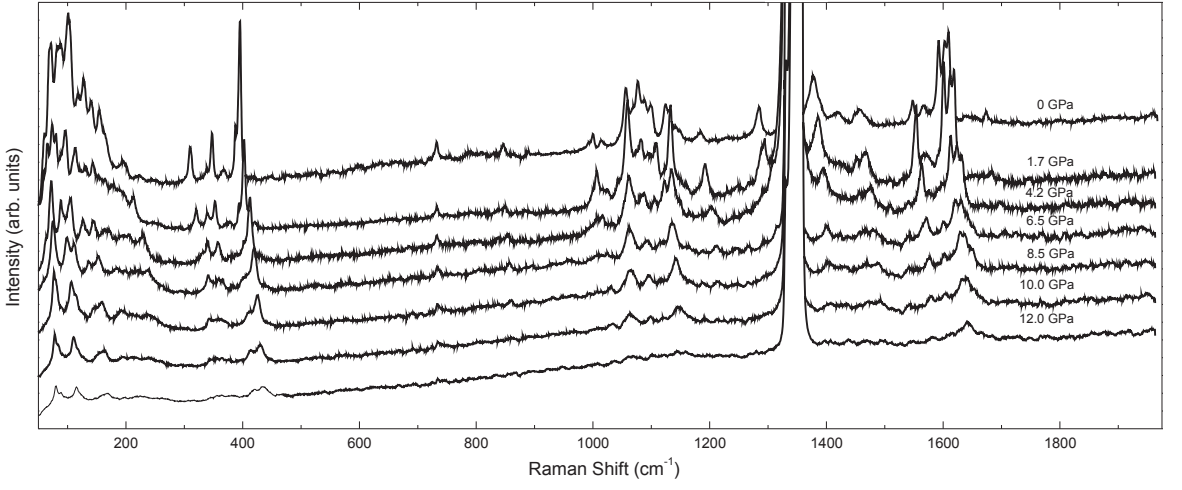
Intensity (arb. units)
0 GPa
1.7 GPa
4.2 GPa
6.5 GPa
8.5 GPa
10.0 GPa
12.0 GPa
200
400
600
800
1000
1200
1400
1600
1800
Raman Shift (cm-1)

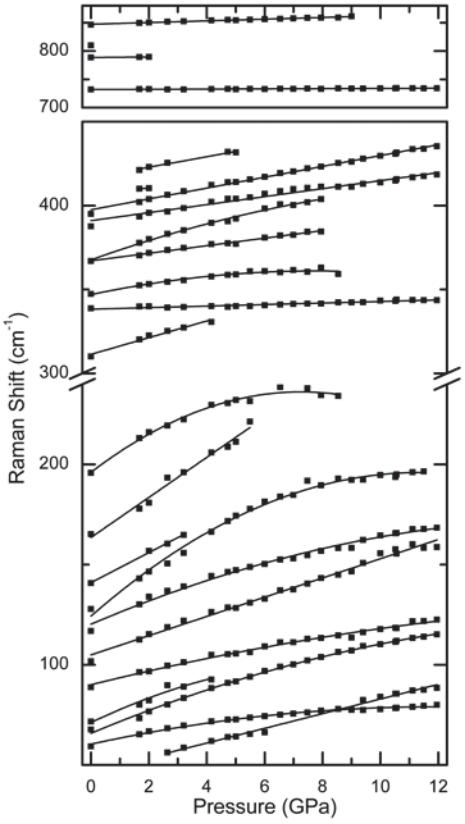
Raman Shift (cm-1)
800
700
400
300
200
100
0
2
4
6
8
10
12
Pressure (GPa)

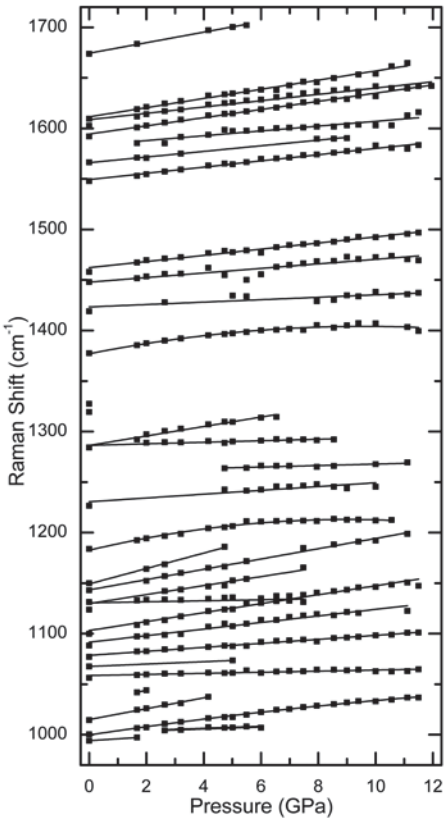
Raman Shift (cm-1)
1700
1600
1500
1400
1300
1200
1100
1000
0
2
4
6
8
10
12
Pressure (GPa)

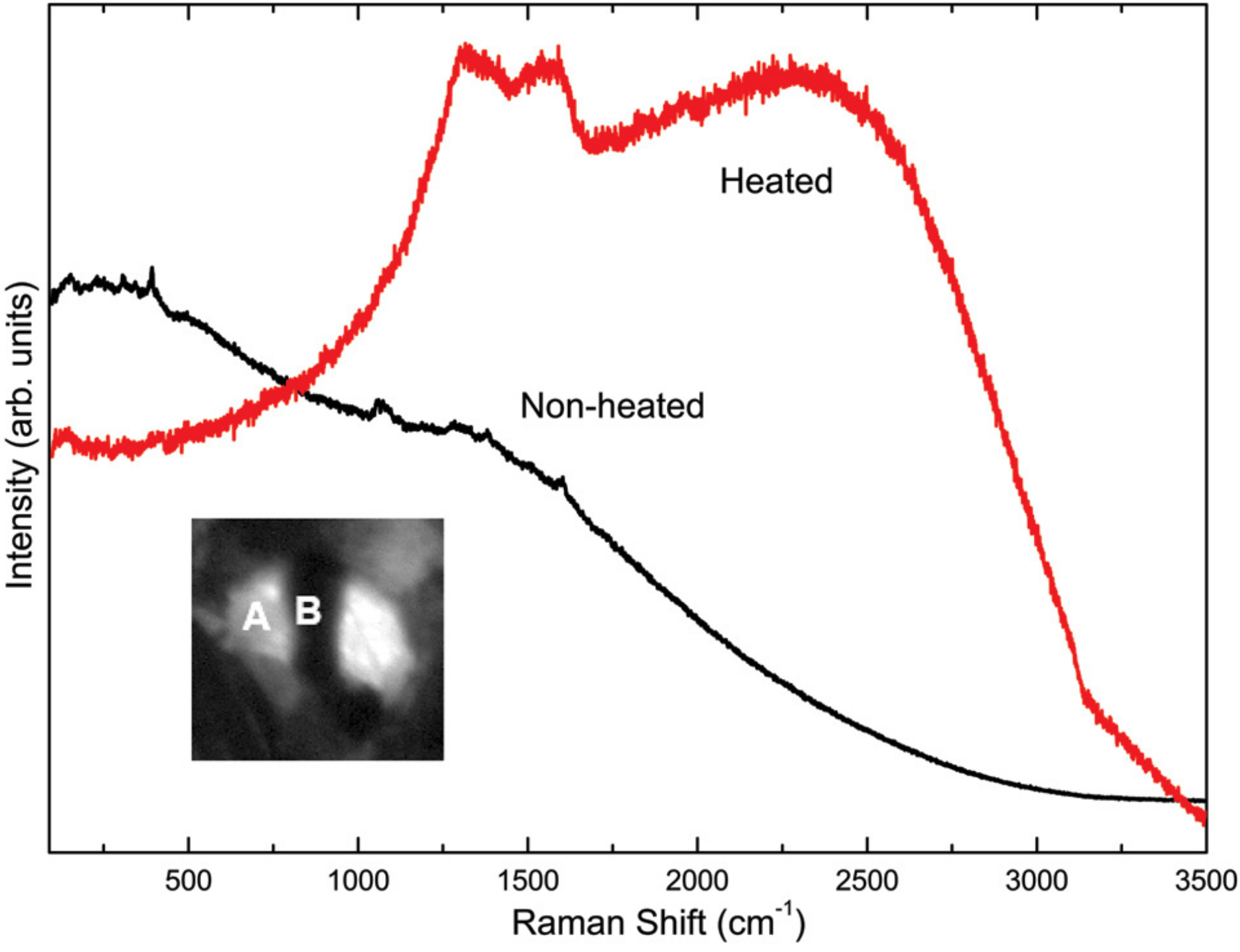
Heated
Non-heated
A
B
Intensity (arb. units)
500
1000
1500
2000
2500
3000
3500
Raman Shift (cm-1)

(a)

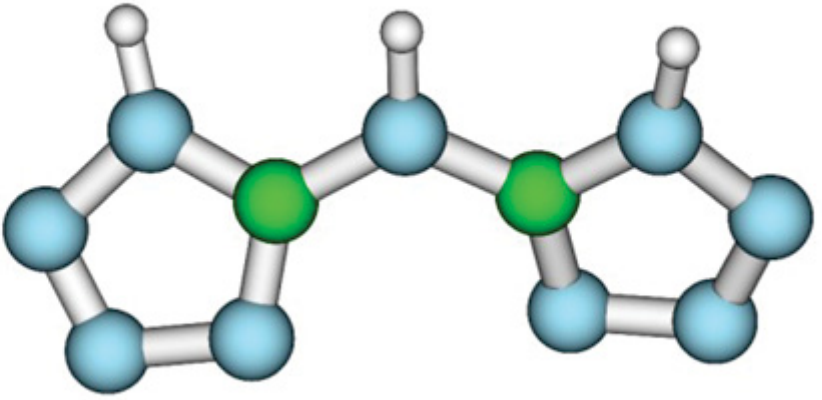

(b)

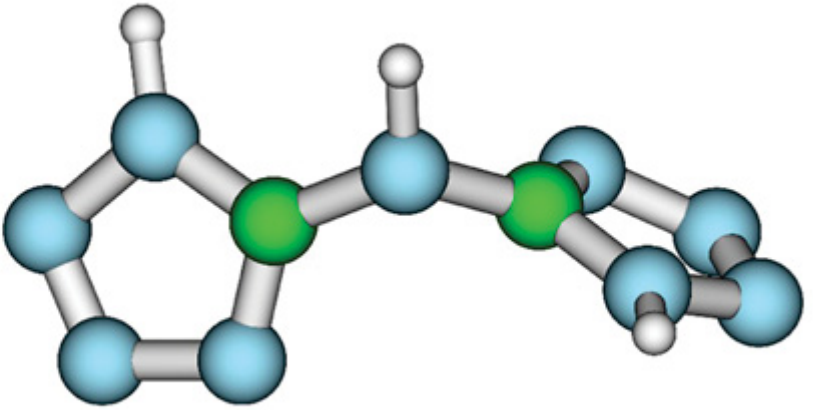

(c)